25th ABCM International Congress of Mechanical Engineering
October 20-25, 2019, Uberlândia, MG, Brazil

COB-2019-0205
ERROR ANALYSIS IN FLUID-STRUCTURE INTERACTION PROBLEMS, WITH FULLY EULERIAN FORMULATION, VIA FINITE ELEMENT METHOD

Daniel Coradini Schwarz
Hilbeth Parente Azikri de Deus
Universidade Tecnológica Federal do Paraná - Av. Sete de Setembro 3165, CEP 80230-901, Curitiba - PR - Brasil
danielcschwarz@gmail.com; azikri@utfpr.edu.br;

Abstract. *It is presented, in this paper, an error analysis for adaptive finite element approximation of fluid-structure interaction problems. A monolithic fully Eulerian formulation with conforming mesh is employed. In this work bi-dimensional domains, incompressible neo-Hookean solids and incompressible Newtonian fluids are considered. The error analysis is based on a dual weighted residual method and the a posteriori error estimate is derived from it. This estimate is employed as a criteria for the implementation of a h-adaptive mesh refinement, which is done through a red-green-blue algorithm. A numerical example is analyzed. The formulation proposed solves the problem correctly, demonstrating the robustness of the chosen FSI method. The adaptive mesh results in a smaller error when compared to an uniformly refined mesh with the same number of elements.*

Keywords: *error estimate, fluid-structure interaction, fully Eulerian, finite element method.*

1. INTRODUCTION

Fluid-Structure Interaction (FSI) is a subject of great importance in many domains, as engineering and biomedical sciences. Problems of this field are complex and non-linear. Also, obtaining experimental results is generally difficult and expensive (Chakrabarti, 2005). This way, numerical approximations are very often the best choice for the evaluation of FSI problems.

The methods for FSI analysis may be divided in two major groups: partitioned and monolithic (Hou *et al.*, 2012). The first equates solid and fluid domains in different structures, in a way that the solid-fluid interface is described explicitly. The second one approaches both domains in a single structure, the solid-fluid interface is described implicitly, which makes for methods that are potentially more precise and robust. The monolithic formulation proposed on this work belongs to the fully Eulerian class, which has brought some attention to it due to its versatility and efficiency (Pironneau, 2016; Richter, 2013).

A further differentiation may be made in regard to the type of mesh: conforming mesh and non-conforming mesh (Hou *et al.*, 2012). The former considers the solid-fluid interface as a physical boundary, requiring the mesh to conform to this interface. Constant mesh updating is needed so that the interface between elements keeps up with the solid-fluid interface movement. The mesh used in this study belongs to this class. Non-conforming meshes treat the boundary location and conditions as constraints imposed to the model. Mesh elements can, this way, be intercepted by the solid-fluid interface and no mesh updating is necessary.

In computer simulations, particularly by Finite Element Methods (FEM), error estimates are indispensable tools for the development of a robust and efficient algorithm (Babuška *et al.*, 1983). They are used to evaluate the accuracy of numerical approximations and also the effectiveness of adaptive meshes. These estimates can be divided in two groups: *a priori* error estimates, which are obtained before any numerical approximation, and *a posteriori* error estimates, which are derived from a previous approximation (Guermond and Ern, 2004). In this study, an *a posteriori* error estimate was determined.

Partial differential equations may have solutions that vary abruptly in small parts of the domain, which leads to adaptive meshes having a efficiency advantage over uniform meshes (Brenner and Scott, 2008). In h-adaptive meshes this is done through the modification of the mesh geometry. On the other hand, p-adaptive methods modify the order of the interpolation polynomials. In hp-adaptive methods a mixed strategy is used.

The h-adaptive method, which was chosen for this study, adapts the mesh through refinement, coarsening or smoothing of the elements (Verfürth, 2013). We employ a method based only on refinement, done with a red-green-blue algorithm (Bartels, 2016).

2. FSI FORMULATION

It is presented, in this section, the balance laws for the FSI problem, the constitutive relationships for solid and fluid media, the strong and weak formulations and the discretized version of the problem. The code implementation for numerical the approach was done in FreeFem++, a free software for resolution of partial differential equations (Hecht, 2012).

2.1 Balance laws

In this context, the derivative operators $\nabla(\ )$, $\nabla\cdot(\ )$ and $\Delta(\ )$ are the gradient, the divergence and the Laplacian, respectively. As the framework is Eulerian, these derivatives are all in respect to spatial coordinate $\boldsymbol{x}$ (and not in respect to reference coordinate $\boldsymbol{X}$, as on a Lagrangian framework).

The FSI problem is obtained from the mass balance and the linear momentum balance equations.

The mass balance is presented in Eq. (1), in which ρ is the density, $\boldsymbol{v}$ is the velocity and $D_t(\ )$ is the total time derivative.

$$D_t\rho - \rho\nabla\cdot\boldsymbol{v} = 0. \tag{1}$$

Equation (2) shows the balance of linear momentum, where $\boldsymbol{T}$ is the Cauchy stress tensor and $\boldsymbol{f}$ is the body force density vector.

$$\rho D_t\boldsymbol{v} - \nabla\cdot\boldsymbol{T} = \rho\boldsymbol{f}. \tag{2}$$

2.2 Constitutive relations

The fluid medium is described in terms of an incompressible Newtonian fluid, by Eq. (3), where p is the pressure, μ is the viscosity, $\boldsymbol{I}$ is the identity matrix and $D(\ ) := \nabla(\ ) + \nabla(\ )^T$.

$$\boldsymbol{T} = -p\boldsymbol{I} + \mu(\rho)D(\boldsymbol{v}). \tag{3}$$

The solid is a incompressible neo-Hookean material, which is described by Eq. (4), where $\boldsymbol{u}$ is the displacement and s is a stiffness parameter, and $\boldsymbol{B}$ is the left Cauchy-Green stain tensor.

$$\boldsymbol{T} = -p\boldsymbol{I} + s\boldsymbol{B}, \tag{4}$$

We aim to describe the solid based on its pressure and displacement, $\boldsymbol{p}$ and $\boldsymbol{u}$. Noting that $\boldsymbol{B} = \boldsymbol{F}\boldsymbol{F}^T$, $\boldsymbol{F}$ being the deformation gradient, and that in the Eulerian frameworks we have $\boldsymbol{F}^{-1} = \boldsymbol{I} - \nabla\boldsymbol{u}$, Eq. (4) may be presented in the form of Eq. (5).

$$\boldsymbol{T} = -p\boldsymbol{I} + s(D(\boldsymbol{u}) - \nabla\boldsymbol{u}^T\nabla\boldsymbol{u}). \tag{5}$$

2.3 Strong form

The global domain (Ω) of the FSI problem is partitioned into a fluid (Ω_f) and a solid (Ω_s) subdomains. The subscripts $(\ )_s$ e $(\ )_f$ are referred to describe properties for the solid and fluid domains, respectively. The subscript $(\ )_0$ makes reference to the initial time, $t = 0$. Equations (6) define the characteristic functions.

$$\chi_f(\boldsymbol{x}) = \begin{cases} 1, \text{ if } \boldsymbol{x} - \boldsymbol{u}(\boldsymbol{x},t) \in \Omega_{f,0}; \\ 0, \text{ if } \boldsymbol{x} - \boldsymbol{u}(\boldsymbol{x},t) \in \Omega_{s,0}\cup\Gamma_{i,0}, \end{cases} \quad ; \quad \chi_s(\boldsymbol{x}) = 1 - \chi_f(\boldsymbol{x}). \tag{6}$$

It's also necessary to define the "convective velocity" $\boldsymbol{w}$, that is an extension of the solid velocity into the fluid domain. It is determined by Eq. (7), where α_w is a small specified constant.

$$\chi_s\,(\boldsymbol{w} - \boldsymbol{v}) - \chi_f\alpha_w\Delta\boldsymbol{w} = \boldsymbol{0} \text{ on } \Omega. \tag{7}$$

It is considered here that the boundaries Γ_N, Γ_D and Γ_i are the Neumann condition boundaries, the Dirichlet condition boundaries and the solid-fluid interface, respectively. The tension vector $\boldsymbol{g}^N$ and the velocity field $\boldsymbol{v}^D$ are prescribed in Γ_N and Γ_D, respectively. In this way, the following strong form for the FSI problem is proposed.

Problem 1 *Strong Form - Find* $(\boldsymbol{v}, p, \boldsymbol{u}, \boldsymbol{w})$ *, so that:*

$$\begin{array}{llll}
\rho D_t\boldsymbol{v} - \nabla\cdot\boldsymbol{T} = \rho\boldsymbol{f} & \text{on } \Omega; & \boldsymbol{w} = \boldsymbol{0} & \text{on } \Gamma_D\cup\Gamma_N; \\
\chi_f\nabla\cdot\boldsymbol{v} = 0 & \text{on } \Omega; & \boldsymbol{u}|_{t=0} = \boldsymbol{0} & \text{on } \Omega; \\
\partial_t\boldsymbol{u} + \boldsymbol{w}\cdot\nabla\boldsymbol{u} - \boldsymbol{w} = \boldsymbol{0} & \text{on } \Omega; & \boldsymbol{v}|_{t=0} = \boldsymbol{v}_0 & \text{on } \Omega; \\
\chi_s\,(\boldsymbol{w} - \boldsymbol{v}) - \chi_f\alpha_w\Delta\boldsymbol{w} = \boldsymbol{0} & \text{on } \Omega; & \boldsymbol{v}_f = \boldsymbol{v}_s & \text{on } \Gamma_i; \\
\boldsymbol{T}\boldsymbol{n} = \boldsymbol{g}^N & \text{on } \Gamma_N; & \boldsymbol{T}_f\boldsymbol{n} = \boldsymbol{T}_s\boldsymbol{n} & \text{on } \Gamma_i; \\
\boldsymbol{v} = \boldsymbol{v}^D & \text{on } \Gamma_D. & &
\end{array} \tag{8}$$

Observation: $(\boldsymbol{v}, p, \boldsymbol{u}, \boldsymbol{w})$ *are defined in* $\{H^2, H^1, H^2, H^2\}$*, where* H^n *is the Sobolev space.*

2.4 Weak form and discretizations

The weak form is obtained from the strong form through integration by parts and the application of Gauss's theorem (Brenner and Scott, 2008). These steps are omitted for sake of simplicity.

The FSI weak formulation must be discretized in time (in transient problems) and space. The time derivatives are performed by finite differences, as usual for transient problems in FEM. There are a variety of methods available for transient approach, some of the most common are: explicit Euler, implicit Euler, Crank-Nicolson, fractional-step θ (Kuzmin, 2010). The implicit Euler method is used here due to its stability and simplicity. The time interval of analysis, $I = (0, T] \subset \mathbb{R}$, is divided in $\mathcal{N}$ time steps, $0 = t^0 < t^1 < t^2 < ... < T$, with $\delta t = t^{n+1} - t^n$.

The space discretization is done via Galerkin FEM, the subscript $(\,)_h$ indicates a quantity discretized on space. The space of functions are presented in Eq. (9), where quadratic elements, $\mathcal{P}_2$, are used for the velocity field and linear triangular elements, $\mathcal{P}_1$, for the pressure field.

$$\begin{aligned}
\mathcal{H}_h &=: \{\boldsymbol{\phi} \in \mathcal{C}(\Omega_h; \mathbb{R}^2);\ \boldsymbol{\phi}|_K \in \mathcal{P}_2(K) \text{ for each } K \in \mathcal{T}_h\};\\
\mathcal{L}_h &=: \{\boldsymbol{\phi} \in \mathcal{C}(\Omega_h);\ \boldsymbol{\phi}|_K \in \mathcal{P}_1(K) \text{ for each } K \in \mathcal{T}_h\};\\
\mathcal{H}_{0h} &=: \{\boldsymbol{\phi} \in \mathcal{H}_h; \boldsymbol{\phi} = \mathbf{0} \text{ on } \Gamma_D\};\\
\mathcal{H}_{Dh} &=: \{\boldsymbol{\phi} \in \mathcal{H}_h; \boldsymbol{\phi} = \boldsymbol{\phi}_D \not\equiv \mathbf{0} \text{ on } \Gamma_D\},
\end{aligned} \tag{9}$$

in which $C(\,)$ is the space of continuum functions.

After some mathematical manipulations, the FSI problem can be presented in a concise form shown in Problem 2.

Problem 2 *Discretized Weak Form - Find* $(\boldsymbol{v}_h^{n+1}, p_h^{n+1}) \in (\mathcal{H}_{Dh}, \mathcal{L}_h)$*, for* $n \in 0..(\mathcal{N}-1)$*, with* $\boldsymbol{v}_h^0 = \boldsymbol{v}_0$*, so that:*

$$\begin{aligned}
&\left(\rho(\boldsymbol{v}_h^{n+1} - \boldsymbol{v}_h^n)/\delta t + \rho(\nabla \boldsymbol{v}_h^{n+1})\boldsymbol{v}_h^n, \boldsymbol{\psi}^v\right)_{\Omega_h^n} - \left(\boldsymbol{T}_h^{n+1}, \nabla \boldsymbol{\psi}^{v_h}\right)_{\Omega_h^n}\\
&= \left(\rho \boldsymbol{f}_h^{n+1}, \boldsymbol{\psi}^v\right)_{\Omega_h^n} + \left(\boldsymbol{g}^N, \boldsymbol{\psi}^v\right)_{\Gamma_{Nh}},\ \forall \boldsymbol{\psi}^v \in \mathcal{H}_{0h};\\
&\left(\nabla \cdot \boldsymbol{v}_h^{n+1}, \psi^p\right)_{\Omega_h^n} = 0,\ \forall \psi^p \in \mathcal{L}_h,
\end{aligned} \tag{10}$$

where $\boldsymbol{\psi}^v, \boldsymbol{\psi}^u, \boldsymbol{\psi}^w$ and ψ^p are the test functions.

The displacement on the solid domain is computed based on the velocity field. Equation (7) determines the nodes displacements on the fluid domain, through the convective velocity. Once all variables are found, the mesh is updated and the next time step is calculated, until the analysis is finished at $t^{n+1} = T$.

3. ERROR ANALYSIS

The Dual Weighted Residual method (DWR method) is well established for error analysis and has been used in similar studies, as in Richter and Wick (2015). Thus, it was chosen for this work.

3.1 Dual Weighted Residual method

We initially rewrite Problem 2 in a compact form, shown in Problem 3.

Problem 3 *- Find* $\boldsymbol{U} \in \{\mathcal{X} + \boldsymbol{U}^D\}$ *so that*

$$\mathfrak{A}(\boldsymbol{U}, \boldsymbol{\psi}) = 0,\ \forall \boldsymbol{\psi} \in \mathcal{X}, \tag{11}$$

in which $\boldsymbol{U}$ *is the vector of variables,* $\boldsymbol{\psi}$ *is a vector of test functions and* $\mathcal{X}$ *is an adequate function space.*

The Galerkin approximation is:

Problem 4 *- Find* $\boldsymbol{U}_h \in \{\mathcal{X}_h + \boldsymbol{U}_h^D\}$ *so that*

$$\mathfrak{A}(\boldsymbol{U}_h, \boldsymbol{\psi}) = \mathbf{0},\ \forall \boldsymbol{\psi} \in \mathcal{X}_h, \tag{12}$$

in which $\boldsymbol{U}_h$ *is the vector of variables,* $\mathcal{X}_h$ *is an adequate function space.*

The directional derivative (Gâteaux derivative) is defined in Eq. (13), as it is necessary for the following analysis. The derivatives for the whole formulation are not shown here. These and other steps, that are omitted here for simplicity, can be found in Schwarz (2018).

$$\mathfrak{A}'(\boldsymbol{U}, \boldsymbol{\psi}; \boldsymbol{\Phi}) = \frac{d}{d\epsilon}\mathfrak{A}(\boldsymbol{U} + \epsilon\boldsymbol{\Phi})(\boldsymbol{\psi})\bigg|_{\epsilon=0} \tag{13}$$

We consider a goal oriented problem, which consists in the minimization of a functional of interest $J(\ )$. It is defined the following Lagrangian function $\mathscr{L}(\boldsymbol{U},\boldsymbol{Z}) = J(\boldsymbol{U}) - \mathfrak{A}(\boldsymbol{U},\boldsymbol{Z})$, where $\boldsymbol{Z}$ is a vector of dual variables.

The derivative of $\mathscr{L}$ with respect to $\boldsymbol{Z}$ in the direction $\boldsymbol{\psi}$ gives the primal problem:

$$\mathscr{L}'(\boldsymbol{U},\boldsymbol{Z};\boldsymbol{\psi}) = -\mathfrak{A}(\boldsymbol{U},\boldsymbol{\psi}) = 0,\ \forall \boldsymbol{\psi} \in \mathcal{X}. \tag{14}$$

By the other hand, the derivative of $\mathscr{L}$ with respect to $\boldsymbol{U}$ in the direction $\boldsymbol{\Phi}$, results in the dual problem:

$$\mathscr{L}'(\boldsymbol{U},\boldsymbol{Z};\boldsymbol{\Phi}) = J'(\boldsymbol{U};\boldsymbol{\Phi}) - \mathfrak{A}'(\boldsymbol{U},\boldsymbol{Z};\boldsymbol{\Phi}) = 0,\ \forall \boldsymbol{\Phi} \in \mathcal{X}. \tag{15}$$

The error $J(\boldsymbol{U}) - J(\boldsymbol{U}_h)$ can then be expressed by Eq. (16).

$$J(\boldsymbol{U}) - J(\boldsymbol{U}_h) = \mathscr{L}(\boldsymbol{U},\boldsymbol{Z}) - \mathscr{L}(\boldsymbol{U}_h,\boldsymbol{Z}_h). \tag{16}$$

Proposition 1 *Let $L(\ )$ be a functional defined on $\mathcal{X}$, three times Gâteaux differentiable and with a stationary point $x \in \mathcal{X}$, then*

$$L'(x,\psi) = 0,\ \forall \psi \in \mathcal{X}. \tag{17}$$

Let $\mathcal{X}_h$ be a finite dimensional subspace of $\mathcal{X}$. The Galerkin approximation is:

$$L'(x_h,\psi_h) = 0,\ \forall \psi_h \in \mathcal{X}_h, \tag{18}$$

in which $x_h \in \mathcal{X}_h$ is the discrete solution. This way, we obtain the following expression for the error on the functional $L(\ )$:

$$L(x) - L(x_h) = \frac{1}{2}L'(x_h, x - \psi_h) + \mathcal{R}_h,\ \forall \psi_h \in \mathcal{X}_h, \tag{19}$$

in which the remainder $\mathcal{R}_h$ is cubic on the error $e = x - x_h$.

The error representation obtained can be expressed in terms of the primal and dual remainders through Proposition 2.

Proposition 2 *Let $(\boldsymbol{U},\boldsymbol{Z})$ and $(\boldsymbol{U}_h,\boldsymbol{Z}_h)$ be solutions of Eqs.* (17) *and* (18)*, respectively. Then it follows that:*

$$J(\boldsymbol{U}) - J(\boldsymbol{U}_h) = \frac{1}{2}\varrho(\boldsymbol{U},\boldsymbol{Z} - \boldsymbol{\psi}_h) + \frac{1}{2}\varrho^*(\boldsymbol{U}_h,\boldsymbol{U} - \boldsymbol{\Phi}_h;\boldsymbol{Z}_h) + \mathcal{R}_h'''\ \forall(\boldsymbol{\Phi}_h,\boldsymbol{\psi}_h) \in \mathcal{X}_h \times \mathcal{X}_h, \tag{20}$$

with the following primal and dual remainders:

$$\begin{aligned} &\varrho(\boldsymbol{U}_h,\cdot) = -\mathfrak{A}(\boldsymbol{U}_h,\cdot);\\ &\varrho^*(\boldsymbol{U}_h,\boldsymbol{Z}_h;\cdot) = J'(\boldsymbol{U}_h;\cdot) - \mathfrak{A}'(\boldsymbol{U}_h,\boldsymbol{Z}_h;\cdot). \end{aligned} \tag{21}$$

Where the remainder $\mathcal{R}_h'''$, is cubic on the primal and dual error $\mathbf{e} = \{\boldsymbol{E},\boldsymbol{E}^*\} = \{\boldsymbol{U} - \boldsymbol{U}_h, \boldsymbol{Z} - \boldsymbol{Z}_h\}$.

Some considerations are made at this point so that we are able to go further with the analysis.

- $\mathcal{R}_h'''$ is neglected;
- It is noted that a stabilization term could be added if necessary, it is not the case for proposed FSI formulation.
- The local projection scheme is "weakly consistent", which means that when the strong solution $\{\boldsymbol{U};\boldsymbol{Z}\}$ is applied, there is still an error of the same order of the discretization.
- The terms $\boldsymbol{U} - \boldsymbol{\Phi}_h$ e $\boldsymbol{Z} - \boldsymbol{\psi}_h$ are approximated by, respectively, $I''_{Zh}\boldsymbol{U}_h - \boldsymbol{U}_h$ and $I''_{Zh}\boldsymbol{Z}_h - \boldsymbol{Z}_h$, so that we have

  $$J(\boldsymbol{U}) - J(\boldsymbol{U}_h) \approx \breve{E}(\boldsymbol{U}_h,\boldsymbol{Z}_h), \tag{22}$$

  in which

  $$\breve{E}(\boldsymbol{U}_h,\boldsymbol{Z}_h) := \frac{1}{2}\varrho(\boldsymbol{U}_h, I''_{Zh}\boldsymbol{Z}_h - \boldsymbol{Z}_h) + \frac{1}{2}\varrho^*(\boldsymbol{U}_h,\boldsymbol{Z}_h, I''_{Zh}\boldsymbol{U}_h - \boldsymbol{U}_h), \tag{23}$$

  and I''_{Zh} is an higher order interpolant of the bilinear solution.

The error representation can be simplified with a relation between the primal and dual remainders shown in Proposition 3.

Proposition 3 *Let $\Delta\varrho$ be a remainder defined by:*

$$\begin{aligned}&\min_{\boldsymbol{\varphi}\in\mathcal{X}_h}\varrho^*(\boldsymbol{U}_h,\boldsymbol{Z}_h,\boldsymbol{U}-\varphi_h)=\min_{\boldsymbol{\varphi}\in\mathcal{X}_h}\varrho(\boldsymbol{U}_h,\boldsymbol{Z}-\boldsymbol{\varphi}_h)+\Delta\varrho;\\&\Delta\varrho=\int_0^1\left[\mathfrak{A}''(\boldsymbol{U}_h+s\boldsymbol{E},\boldsymbol{Z}_h+s\boldsymbol{E}^*;\boldsymbol{E},\boldsymbol{E})-J''(\boldsymbol{U}_h+s\boldsymbol{E};\boldsymbol{E},\boldsymbol{E})\right]ds.\end{aligned}\tag{24}$$

This way, we obtain the following representation for the error on functional $J(\,)$:

$$J(\boldsymbol{U})-J(\boldsymbol{U}_h)=\min_{\boldsymbol{\varphi}\in\mathcal{X}_h}\varrho(\boldsymbol{U}_h,\boldsymbol{Z}-\boldsymbol{\varphi})+\mathcal{R}_h'',\tag{25}$$

in which the remainder $\mathcal{R}_h''$ is quadratic on the error.

We note that the existence of solution for the primal and dual problems is not assured. This is a non-trivial task and few studies with this result are available on the literature. On the present context, the Gâteaux derivative does not need to be exact, it needs only to be sufficiently well behaved so that the convergence by the Newton method is achieved. The precision of the approximate solution for the primal problem is evaluated through the residue. It is not possible to do the same for the dual problem though, we note this issue happens on similar analysis for any non-linear problem.

Further analysis allow us to write Eq. (25) as Eq. (26). The remainder can be neglected due to the linearity of the bilinear operator $\mathfrak{A}(\cdot,\cdot)$ and the functional $J(\,)$.

$$J(\boldsymbol{U})-J(\boldsymbol{U}_h)\approx\varrho(\boldsymbol{U}_h,\boldsymbol{Z}-\boldsymbol{\varphi}_h)=\mathfrak{A}(\boldsymbol{U}_h,\boldsymbol{Z}-\boldsymbol{\varphi}_h).\tag{26}$$

Due to the coercivity of $\mathfrak{A}(\cdot,\cdot)$ we have Eq. (27), in which $\|\cdot\|_E$ is the energy norm.

$$\|\boldsymbol{a}-\boldsymbol{b}\|_E\leq c_m\sup_{\mathcal{Z}\in\mathcal{X},\|\mathcal{Z}\|=1}|\mathfrak{A}(\boldsymbol{a},\boldsymbol{Z})-\mathfrak{A}(\boldsymbol{b},\boldsymbol{Z})|,\ \forall\boldsymbol{a},\boldsymbol{b}\in\mathcal{X},\tag{27}$$

This way we obtain, through the Galerkin orthogonality, the functional error bounds in terms of the residual, as given in Eq. (28).

$$\|\boldsymbol{e}_h\|_E\leq C\sup_{\mathcal{Z}\in\mathcal{X},\|\mathcal{Z}\|=1}|\min_{\boldsymbol{\varphi}_h\in\mathcal{X}_h}\varrho(\boldsymbol{U}_h,\boldsymbol{Z}-\boldsymbol{\varphi}_h)|\leq C\sup_{\mathcal{Z}\in\mathcal{X},\|\mathcal{Z}\|=1}|\varrho(\boldsymbol{U}_h,\boldsymbol{Z}-\boldsymbol{\varphi}_h)|,\tag{28}$$

3.2 Fluid and Solid Analysis

The fluid constitutive relation (3) allow us to write Eq. (29) for the fluid domain.

$$(\nabla p,\boldsymbol{\psi}^v)_{\Omega_f}+\rho_f\left(\partial\boldsymbol{v}/\partial t,\boldsymbol{\psi}^v\right)_{\Omega_f}+\mu\left(\Delta\boldsymbol{v},\boldsymbol{\psi}^v\right)_{\Omega_f}+\rho_f\left((\nabla\boldsymbol{v})\boldsymbol{v},\boldsymbol{\psi}^v\right)_{\Omega_f}=0.\tag{29}$$

For an specific element "K" of the mesh and a specified time step t^{n+1} the following error term can be considered.

$$\begin{aligned}\varrho_f^K=&\rho_f\left(\partial\boldsymbol{v}_h/\partial t,\boldsymbol{\psi}^v\right)_K+\rho_f\left((\nabla\boldsymbol{v}_h)\boldsymbol{v}_h,\boldsymbol{\psi}^v\right)_K+\mu\left(\nabla\boldsymbol{v}_h,\nabla\boldsymbol{\psi}^v\right)_K\\=&\rho_f\left(D_t\boldsymbol{v}_h,\boldsymbol{\psi}^v\right)_K+\mu\left(\nabla\boldsymbol{v}_h,\nabla\boldsymbol{\psi}^v\right)_K.\end{aligned}\tag{30}$$

Again, by the Navier-Stokes relation we have:

$$\rho_f\left(D_t\boldsymbol{v}/\partial t,\boldsymbol{\psi}^v\right)_K=-\mu\left(\nabla\boldsymbol{v},\nabla\boldsymbol{\psi}^v\right)_K.\tag{31}$$

This way,

$$\begin{aligned}&\rho_f\left(\partial\boldsymbol{v}_h/\partial t,\boldsymbol{\psi}^v\right)_K\leq-\mu\left(\nabla\boldsymbol{v},\nabla\boldsymbol{\psi}^v\right)_K+|\mu\left(\nabla\boldsymbol{v},\nabla\boldsymbol{\psi}^v\right)_K|;\\&\therefore\rho_f\left(\partial\boldsymbol{v}_h/\partial t,\boldsymbol{\psi}^v\right)_K\leq2|\mu\left(\nabla\boldsymbol{v},\nabla\boldsymbol{\psi}^v\right)_K|.\end{aligned}\tag{32}$$

The term ϱ_1^K can be bounded through the following inequalities:

$$\begin{aligned}|\varrho_1^K|&\leq\rho_f|(D_t\boldsymbol{v},\boldsymbol{\psi}^v)_K|+\mu|(\nabla\boldsymbol{v}_h,\nabla\boldsymbol{\psi}^w)_K|\\&\leq3\mu|(\nabla\boldsymbol{v}_h,\nabla\boldsymbol{\psi}^w)_K|\\&\leq3\mu\|\nabla\boldsymbol{v}_h\|_{L^2(K)}\|\nabla\boldsymbol{\psi}^w\|_{L^2(K)}.\end{aligned}\tag{33}$$

Also, considering that $\exists\, C' > 0$ so that $\|\nabla \boldsymbol{\psi}^w\|_{L^2(K)} < 0$,

$$|\varrho_1^K| \leq 3\mu C' \|\nabla \boldsymbol{v}_h\|_{L^2(K)} \leq 3\mu C' \|\boldsymbol{v}_h\|_{H^2(K)}. \tag{34}$$

The trace theorem (Dobrowolski, 2006) says that $\exists\, C'' > 0$ so that

$$\|v_h\|_{H^2(K)} \leq C'' \|(\nabla v_h)\hat{\boldsymbol{n}}\|_{H^{1/2}(\Gamma_f^K)}, \tag{35}$$

in which $\boldsymbol{n}$ is the unitary vector normal to the element edge and Γ_f^K is the element boundary. This way,

$$\begin{aligned} |\varrho_1^K| \leq & 2\mu C' C'' \|(\nabla v_h)\hat{\boldsymbol{n}}\|_{H^{1/2}(\Gamma_f^K)}; \\ \sum_K |\varrho_1^K| \leq & 2\mu C' C'' \sum_K \|(\nabla v_h)\hat{\boldsymbol{n}}\|_{H^{1/2}(\Gamma_f^K)}; \\ \therefore \|\varrho_1\| \leq & C_1 \sum_K \|(\nabla v_h)\hat{\boldsymbol{n}}\|_{H^{1/2}(\Gamma_f^K)}, \end{aligned} \tag{36}$$

in which $\|\varrho_1\| = \sum_K |\varrho_1^K|$ and $H^{1/2}$ is a fractional Sobolev function space.

This gives us a form for the error on the fluid domain. A similar analysis for the solid domain says that $\exists\, C_2 > 0$, so that:

$$\sum_K |\varrho_2^K| = \|\varrho_2\| \leq C_2 \sum_K \|\boldsymbol{T}_h \hat{\boldsymbol{n}}\|_{H^{1/2}(\Gamma_s^K)}. \tag{37}$$

3.3 FSI *a posteriori* error estimate

Combining Eq. (36) and Eq. (37) a error estimate for the FSI problem is reached, shown in Eq. (38).

$$\|\boldsymbol{e}_h\|_E \leq C_3 \sum_K \|(\nabla \boldsymbol{v}_h)\hat{\boldsymbol{n}}\|_{H^{1/2}(\Gamma_f^K)} + C_4 \sum_K \|\boldsymbol{T}_h \hat{\boldsymbol{n}}\|_{H^{1/2}(\Gamma_s^K)}, \tag{38}$$

in which, C_3 and C_4 are constants.

4. ADAPTIVE MESH

An h-adaptive mesh refinement is used. It is described by the following algorithm, proposed by Guermond and Ern (2004).

Algorithm 1 *- Adaptive Mesh Refinement*

1. *A first coarse mesh, $\mathcal{T}_h^0$, is generated. Iteration counter is set to zero, $i = 0$.*
2. *The FSI problem is resolved for $\mathcal{T}_h^i$, obtaining a solution U^i.*
3. *The local error indicators $e_K^i(U^i, f)$ are calculated for each element $K^i \in \mathcal{T}_h^i$.*
4. *The global error estimate, ε_{global}, is calculated. If it is smaller than L_{global}, the process is ended and U^i is considered the final solution.*
5. *A new mesh is generated. The iteration counter is updated, $i = i + 1$. The process returns to step 2.*

The local error indicators are given by Eq. (39), which is derived from the prior error analysis. The global error is calculated by Eq. (40), where NT is the number of triangles.

$$\varepsilon_{local}(K) = \frac{\|(\nabla \boldsymbol{v})\hat{\boldsymbol{n}}\|_{H_{1/2}(\Gamma_f^K)}}{L_{fluido}} + \frac{\|\boldsymbol{T}\hat{\boldsymbol{n}}\|_{H_{1/2}(\Gamma_s^K)}}{L_{solido}}. \tag{39}$$

$$\varepsilon_{global} = \sqrt{\frac{\sum_{K \in \mathcal{T}_h} (\varepsilon_{local})^2}{NT}}. \tag{40}$$

In step 1 of the Algorithm 1 a initial mesh generation can be done by various methods. In FreeFem++ this is done with a manual input of the number of vertex in each boundary, then the points inside the domains are found with a Voronoi method, and finally the edges are determined with a Delaunay criteria (Owen, 2000). In simple geometries, like the rectangular domains of the numerical example presented on this study, the generation of a first mesh is trivial.

In step 5 of Algorithm 1 the new mesh is generated based on the previous one, with a Red-Green-Blue refinement method. The triangles select through the local indicators are divided. Also, some adjacent triangles are also divided so that mesh quality is preserved (no triangles with angles too large being created). The process is described in a simplified form by Algorithm 2. The exact process is detailed in Schwarz (2018).

Algorithm 2 - *Red-Green-Blue Refinement*

1. *All triangles with $\varepsilon_{local} > 1$ have their three edges marked for refinement.*

2. *Additional edges are marked in a way that no triangle that has an edge marked has its longest edge unmarked.*

3. *Triangles with at least an edge marked are refined as shown by Fig. 1, in accordance to the number of marked edges.*

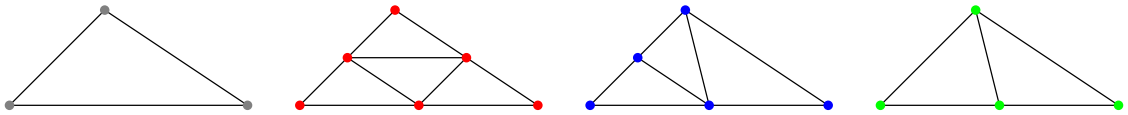

(a) Original triangle (b) Red refinement (c) Blue refinement (d) Green refinement

Figure 1: RGB refinement

Observation: Step 2 of Algorithm 2 is not trivial a new triangle marked this way might generate an additional triangle that has one edge marked having its longest edge unmarked. The complete procedure has to be done in a way to recheck for this adjacent elements.

5. NUMERICAL EXAMPLE

The computational application, presented here, has a square domain described on Fig. 2. The boundaries have null velocity prescribed, except for the upper one, which has a velocity profile given by Eq. (41). This boundary condition causes a circulation of the fluid inside the cavity, which causes a deformation of the solid.

$$\boldsymbol{v}_s(x) = \begin{bmatrix} 4x(1-x) \\ 0 \end{bmatrix}. \tag{41}$$

The simulation parameters and the dimensions of the cavity are presented on Tab. 1.

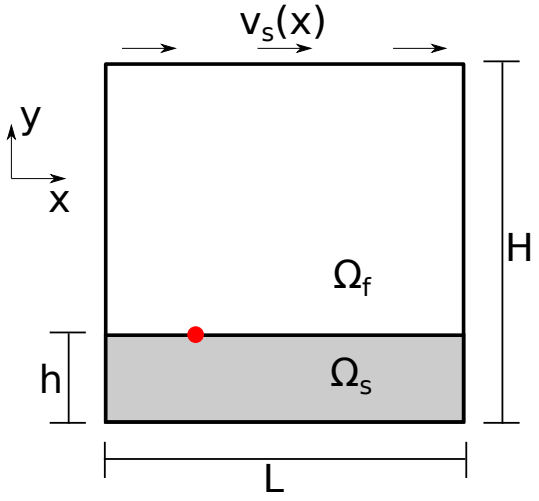

Figure 2: Problem geometry

Table 1: Simulation parameters

Cavity dimensions	
L	1
H	1
h	0.25
Constitutive parameters	
ρ_f	1
μ	0.01
ρ_s	1
s_1	0.05
Adaptivity parameters	
L_{solid}	1e-6
L_{fluid}	1e-3
L_{global}	1.2

The simulation is done with the adaptive mesh refinement approach proposed and also with an uniform mesh refinement procedure, for comparison. The initial mesh is shown in Fig. 3, the local error obtained during the first iteration is in Fig. 4. The triangles selected for refinement are the ones with a ε_{local} greater than one. All triangles are refined in the first iteration, as the initial mesh is very coarse.

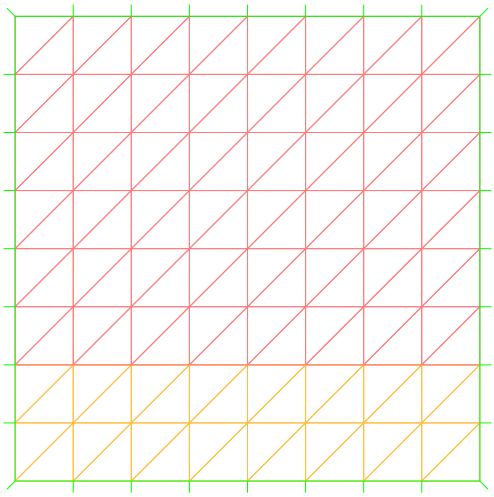

Figure 3: Initial mesh

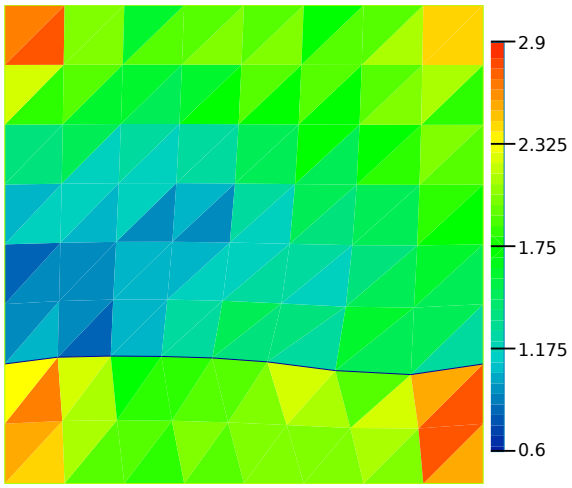

Figure 4: Local error - $log(\varepsilon_{local})$

Figure 6 shows the magnitude of the velocity obtained with the finest adaptive mesh, which is in Fig. 5. It can be noted that this final mesh is finer where the local errors shown in Fig. 4 are higher, as should be expected.

The velocity for the fluid domain shows the circulation of the fluid around an "eye" at about the center of the cavity. The solid domain has no velocity as this is a steady-state example, the deformed solid-fluid interface can also be seen on Fig. 6.

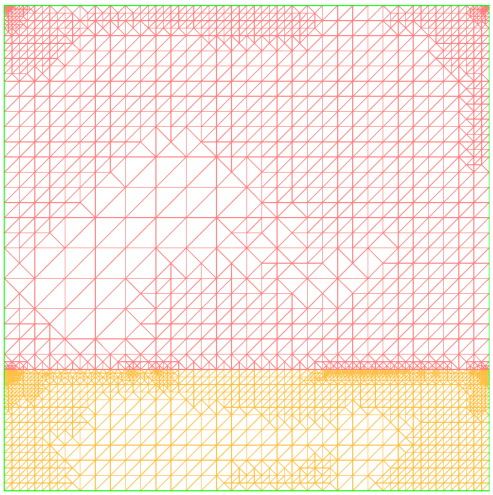

Figure 5: Final adaptive mesh

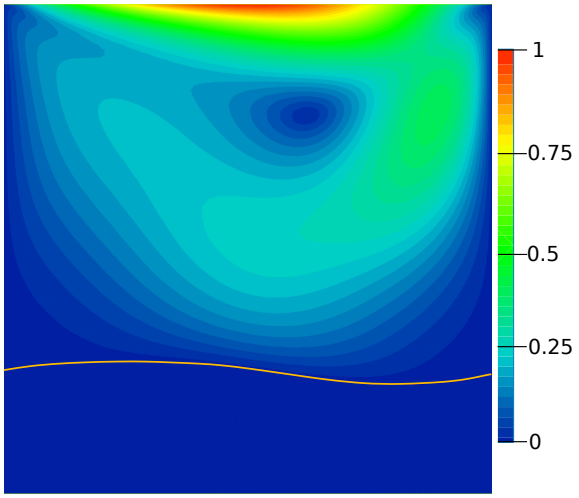

Figure 6: Velocity field

We also observe the displacement $\tilde{\boldsymbol{u}}$ of the point with material coordinates given in Eq. (42), note that the point referenced is on the solid domain. It is also highlighted in red on Fig. 2.

$$\tilde{\boldsymbol{u}}(1/4; 1/4) = \begin{bmatrix} U_x \\ U_y \end{bmatrix} \tag{42}$$

The displacement for each mesh simulated is shown in Tab. 2. They are compared to a result obtained by Richter (2013). We note that the problem geometry and constitutive parameters are identical, so that the comparison is valid.

Table 2: Displacement

Adaptive			Uniform		
NT	U_x	U_y	NT	U_x	U_y
128	-2.8598	1.6628	128	-2.8598	1.6628
512	-2.8236	1.817	512	-2.8236	1.817
1826	-2.8261	1.9258	2048	-2.8263	1.9255
3255	-2.8221	1.9846	8192	-2.8265	1.9802
3977	-2.8185	2.0085	32768	-2.8262	2.0073
4639	-2.8371	2.0101			
Literature result					
$\approx$ 1e6	-2.8244	2.0510			

The global error for each iteration is in Fig. 7. The error is smaller on finer meshes for both refinement methods. However, it is important to stand out that the adaptive refinement gives a lower error for a mesh with similar number of elements (NT).

Figure 8 shows the simulation times, for each iteration. The first two iterations have the same result for both refinement methods, as the initial mesh is the same and the adaptive mesh refinement ended up refining all elements in the first iteration. The following iterations show the advantage obtained with an adaptive mesh refinement in terms of reduction in simulation time.

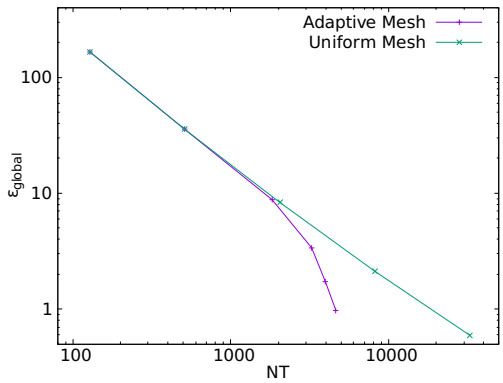

Figure 7: Global error

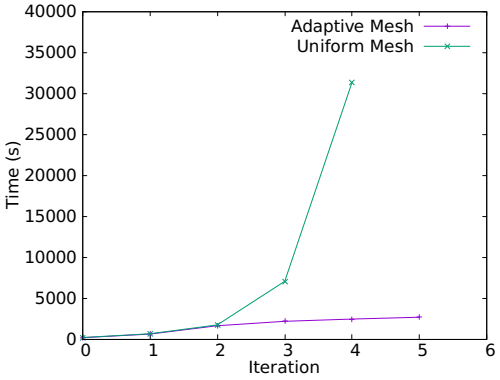

Figure 8: Simulation time per iteration

6. CONCLUSION

In this study, a numerical approach for FSI problems via a fully Eulerian formulation was proposed. An error analysis was developed through an dual weighted residual method. The main steps and considerations were presented and the final result is an *a posteriori* error estimate for the FSI problem.

An adaptive mesh was implemented based on the error estimate proposed. The domains are bi-dimensional with triangular elements and the refinement is h-adaptive, done through a red-green-blue method. This method showed to be robust and did not generate distorted triangles, once the code was properly implemented no issues where encountered on this step of analysis.

A numerical example was presented and it was verified that the FSI formulation is adequate. The results were compared to ones available in the literature and only small differences were observed. Also the adaptive mesh achieved an efficiency gain when compared to an uniform refinement, which shows the efficacy of the adaptive mesh and indirectly of the error estimate used in it.

7. REFERENCES

Babuška, I., Chandra, J. and Flaherty, J.E., 1983. *Adaptive Computational Methods for Partial Differential Equations*. SIAM, Philadelphia.

Bartels, S., 2016. *Numerical Approximation of Partial Differential Equations*. Springer International Publishing, New York, 1st edition.

Brenner, S.C. and Scott, L.R., 2008. *The Mathematical Theory of Finite Element Methods*. Springer-Verlag, New York.

Chakrabarti, S.K., 2005. *Numerial Models in Fluid-Structure Interaction*. WIT, Southampton.

Dobrowolski, M., 2006. *Angewandte Funktionalanalysis: Funktionalanalysis, Sobolev-Räume und elliptische Differentialgleichungen*. Springer-Verlag, Berlin Heidelberg.

Guermond, J. and Ern, A., 2004. *Theory and practice of finite elements*. Springer-Verlag, New York.

Hecht, F., 2012. "New development in FreeFem++". *Journal of Numerical Mathematics*, Vol. 20, No. 3-4, pp. 251–265.

Hou, G., Wang, J. and Layton, A., 2012. "Numerical methods for fluid-structure interaction - a review". *Communications in Computational Physics*, Vol. 12, pp. 337–377.

Kuzmin, D., 2010. *A Guide to Numerical Methods for Transport Equations*. Friedrich-Alexander-Universität, Nürnberg.

Owen, S.J., 2000. "A survey of unstructured mesh generation technology". *7th International Meshing Roundtable*, Vol. 3, pp. 239–267.

Pironneau, O., 2016. "Numerical study of a monolithic fluid-structure formulation". In A. Frediani, B. Mohammadi, O. Pironneau and V. Cipolla, eds., *Variational Analysis and Aerospace Engineering: Mathematical Challenges for the Aerospace of the Future*, Springer, Cham, Vol. 116, pp. 401–120.

Richter, T., 2013. "A fully Eulerian formulation for fluid-structure interaction problems". *Journal of Computational Physics*, Vol. 233, pp. 227–240.

Richter, T. and Wick, T., 2015. "Variational localizations of the dual weighted residual estimator". *Journal of Computational and Applied Mathematics*, Vol. 279, pp. 192–208.

Schwarz, D.C., 2018. *Error estimate analysis applied to Fluid-Structure Interaction problems, with fully Eulerian formulation, via Finite Element Method*. Master's thesis, Universidade Tecnológica Federal do Paraná, Curitiba, Brazil.

Verfürth, R., 2013. *A posteriori error estimation techniques for finite element methods*. Oxford University, Oxford.